

Structure of a pancreatic α -amylase bound to a substrate analogue at 2.03 Å resolution

MINXIE QIAN,^{1,3} SILVIA SPINELLI,¹ HUGUES DRIGUEZ,² AND FRANÇOISE PAYAN¹

¹AFMB-IBSM-CNRS 31 Chemin Joseph Aiguier 13402 Marseille CEDEX 20, France

²Centre de Recherches sur les Macromolécules Végétales, CNRS, B.P. 53, F-38041, Grenoble, France

³Institute of Physical Chemistry Peking University, Beijing 100871, People's Republic of China

(RECEIVED March 3, 1997; ACCEPTED July 9, 1997)

Abstract

The structure of pig pancreatic α -amylase in complex with carbohydrate inhibitor and proteinaceous inhibitors is known but the successive events occurring at the catalytic center still remain to be elucidated. The X-ray structure analysis of a crystal of pig pancreatic α -amylase (PPA, EC 3.2.1.1.) soaked with an enzyme-resistant substrate analogue, methyl 4,4'-dithio- α -maltotrioside, showed electron density corresponding to the binding of substrate analogue molecules at the active site and at the "second binding site." The electron density observed at the active site was interpreted in terms of overlapping networks of oligosaccharides, which show binding of substrate analogue molecules at subsites prior to and subsequent to the cleavage site. A weaker patch of density observed at subsite -1 (using a nomenclature where the site of hydrolysis is taken to be between subsites -1 and +1) was modeled with water molecules. Conformational changes take place upon substrate analogue binding and the "flexible loop" that constitutes the surface edge of the active site is observed in a specific conformation. This confirms that this loop plays an important role in the recognition and binding of the ligand. The crystal structure was refined at 2.03 Å resolution, to an *R*-factor of 16.0 (R_{free} , 18.5).

Keywords: α -amylase; substrate analogue; thiooligosaccharides; X-ray structure

Alpha-amylase (α -1,4 glucan-4-glucanohydrolase, EC 3.2.1.1) catalyses the hydrolysis of α -(1,4) glycosidic linkages of starch components, glycogen, and various oligosaccharides. α -amylase is a member of glycosyl hydrolase family 13, which also contains cyclodextrin glucanotransferases (CGTases) and pullulanases (Henrissat, 1991).

In mammals, α -amylase is present in both salivary and pancreatic secretions. Amino acid sequence comparisons have shown that there is a high degree of identity among the porcine, human, mouse, and rat pancreatic amylase (Pasero et al., 1986).

Porcine pancreatic α -amylase (PPA) is an endo-type amylase. It catalyzes the hydrolysis of internal α -(1,4) glucosidic bonds in amylose and amylopectin via a multiple attack process toward the non-reducing end (Robyt & French, 1970; Prodanov et al., 1984). Two isoenzymes (PPA I and II) are known for pig pancreatic α -amylase (Cozzone et al., 1970). They have the same molecular weight but differ slightly in their amino acid compositions and isoelectric points (Kluh, 1981; Pasero et al., 1986; Alkazaz et al., 1996). The overall conformation of the protein is

practically the same in both the PPAI and PPAlI structures (Gilles et al., 1996).

The enzyme requires one essential calcium ion (Vallee et al., 1959; Steer & Levitzki, 1973) to maintain its structural integrity, and it is activated by chloride ions (Levitzki & Steer, 1974); the maximum enzymatic activity occurs at around pH 7 (Wakim et al., 1969; Ishikawa et al., 1993). Based upon kinetic studies of the action pattern (Robyt & French, 1970), it was suggested that the active site of the pig pancreatic α -amylase contains five subsites which are involved in the binding of glucose units, and that the catalytic attack occurs between subsites -1 and +1 as shown in Figure 1A. The maltopentaose and higher maltodextrin molecules are efficient hydrolytic substrates (Robyt & French, 1970). The catalytic efficiency (k_{cat}/K_m) increases with the chain length from $2\text{ M}^{-1}\text{ s}^{-1}$ in the case of maltose up to $1 \times 10^7\text{ M}^{-1}\text{ s}^{-1}$ in that of 410-residue amylose (Marchis-Mouren & Desseaux, 1989). Since methyl α -maltotrioside has a K_i value of 3 mM, the synthesis of methyl 4,4'-dithiomaltotriose was undertaken (Blanc-Muesser et al., 1992). This compound is not hydrolyzed by porcine pancreatic α -amylase and has a K_i of 9 mM (as was to be expected in the case of a thiooligosaccharide; Driguez, 1997).

We previously described the three-dimensional molecular model of PPA (Qian et al., 1993). It should be mentioned that the molecular models for the α -amylases from human pancreas (Brayer et al., 1995) and human salivary (Rathasubbu et al., 1996) recently described are extremely similar to the pig pancreatic molecular

Reprint requests to: Françoise Payan; AFMB-IBSM-CNRS 31 Chemin Joseph Aiguier, 13402 Marseille CEDEX 20, France; e-mail: payan@afmb.cnrs-mrs.fr.

Abbreviations: PPA, pig pancreatic α -amylase; SA, substrate analogue; RMS, root-mean-square; σ , standard deviation. R -factor = $\sum ||F_{obs}|| - |F_{cal}|| / \sum |F_{obs}|$.

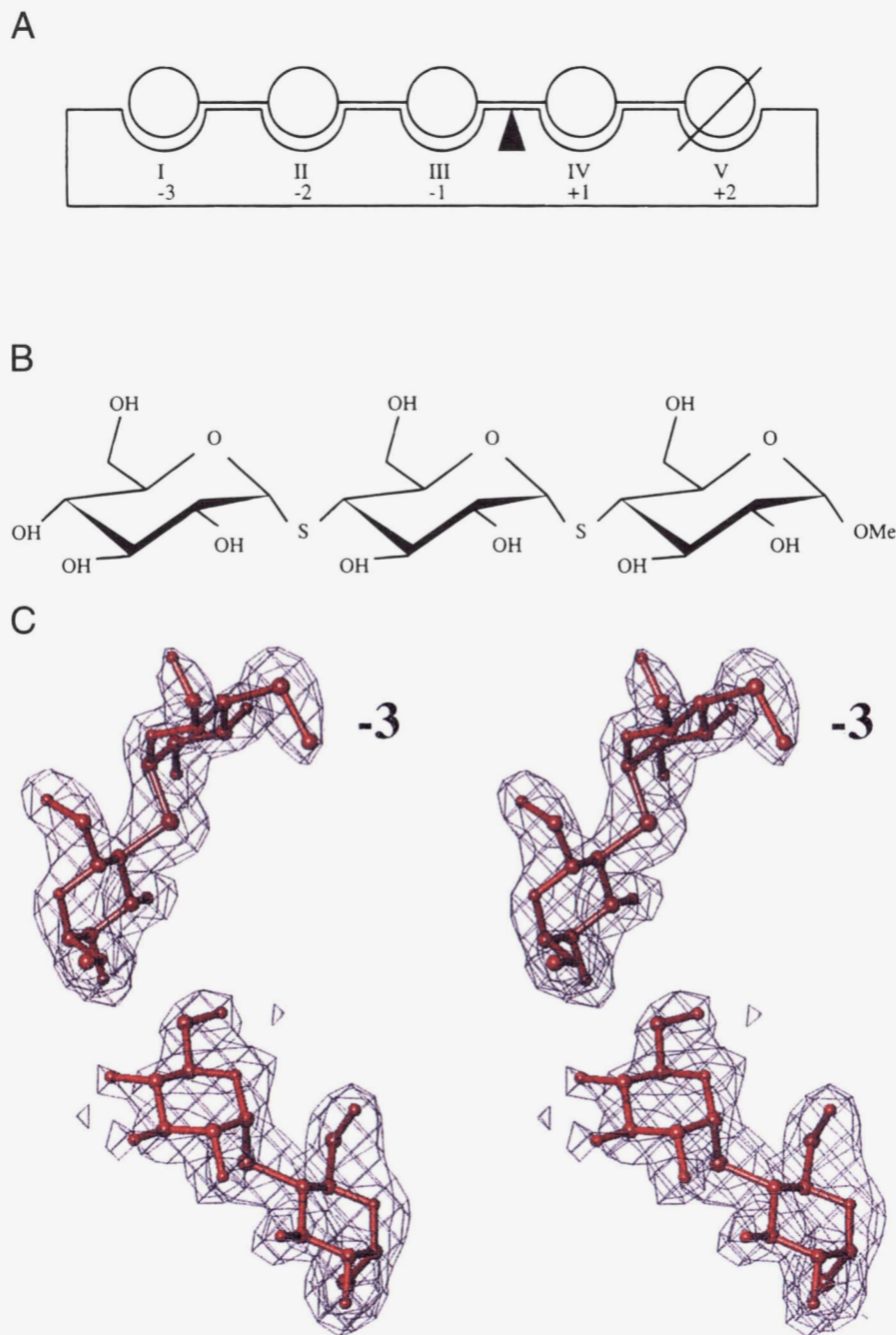


Fig. 1. **A:** Schematic representation of the active site. As in our previous papers, the subsites are numbered I–V working from the nonreducing end. The nomenclature $-n/n+n$, assuming the cleavage to take place between subsites -1 and $+1$ (Davies et al., 1997), was adopted here and has been given in addition. **B:** Structure of the substrate analogue (Blanc-Muesser et al., 1992). **C:** Stereoscopic view of the final $(2F_{obs} - F_{calc}) \exp(i\alpha_{calc})$ electron density map at subsites -3 , -2 , $+1$, and $+2$ at 2.03 Å resolution. The contour is drawn at 1σ level.

model. Crystal structures have been described in other members of glycosyl hydrolase family 13 (Svensson, 1994).

The architecture of the pig pancreatic α -amylase is shown in Figure 2. It is composed of three domains: The central N-terminal domain A, comprising a $(\beta/\alpha)_8$ barrel, contains an extended loop inserted between the third β -strand and the third α -helix (called domain B). The C-terminal domain (domain C) forms a distinct globular unit with 10 β -strands forming a Greek key motif. Ele-

ments from domains A and B are involved in the architecture of the functionally important sites: the active site, the calcium binding site, and the chloride binding site. An atomic description of the interactions between the mammalian enzyme and its inhibitor has been published along with the refined structures of two PPA/acarbose complexes (using two different crystal forms; Qian et al., 1994; Gilles et al., 1996). The X-ray models clearly show that a subset of residues is directly involved in binding the inhibitor and/or

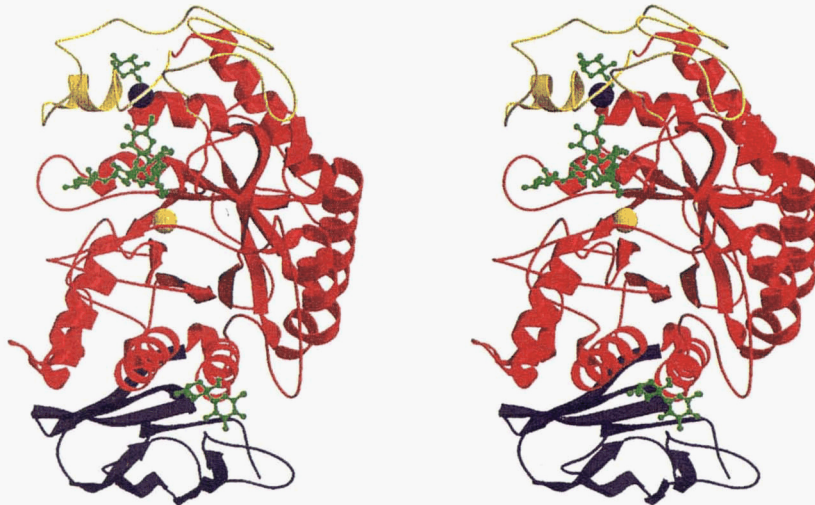


Fig. 2. Stereo MOLSCRIPT (Kraulis, 1991) diagrams of the α -amylase (PPA) structure. The three domains are shown: domain A is colored red; domain B, yellow; domain C, purple. The calcium ion (blue sphere) and the chloride ion (yellow sphere) are also shown in the immediate vicinity of the catalytic center. The acarbose ligand (ball-and-stick representation in green) is bound at the active site cleft. Monosaccharide and disaccharide ligands (in ball-and-stick representation) are shown bound to the surface binding sites.

is in a suitable position to assist the catalysis. The structural arrangement indicates that the requirements for hydrolysis to occur via the general acid hydrolysis mechanism are satisfied in the PPA structure. The widely recognized double-step mechanism originally proposed by Koshland (1953) for retaining glycosyl hydrolases requires the presence of two carboxyl-containing amino acids, the one acting as an acid/base catalyst and the other as the nucleophile responsible for the formation of the glycosyl-enzyme intermediate (McCarter & Withers, 1994). In view of our crystallographic results, we suggested that both Asp197 and Glu233 may be required to produce the β -linked glycosyl-enzyme intermediate. Recent results (McCarter & Withers, 1996) clearly confirm the role of Asp197 as the catalytic nucleophile; Glu233 and Asp300 are hydrogen-bonded to each other via an intervening water molecule (W555) as well as to the glycosidic amine (at the point of cleavage) and may be involved in the acid/base catalysis. The exact role of the other residues present in the mechanism is not yet clear, however.

Two additional carbohydrate binding sites have been identified at the surface of the molecule based on the crystal structure of a complex between PPAI and the substrate maltopentaose (Qian et al., 1995). The maltopentaose complex structure provided evidence that the stability of the structure is enhanced when interactions occur with the substrate and allowed identification of an N-terminal pyrrolidonecarboxylic acid in PPAI.

We recently solved the structure of the pig pancreatic α -amylase in complex with the proteinaceous inhibitor from *Phaseolus vulgaris* (Bompard-Gilles et al., 1996). These data showed that elements from the inhibitor molecule manage to fill the whole substrate-docking region of the PPA and mimic the enzyme-acarbose-ligand interactions.

A number of crystal structures of complexes between members of glycosyl hydrolase family 13 and carbohydrate or proteinaceous inhibitors have now been published. The following studies in particular are worth mentioning in connection with pig pancreatic α -amylase: its complex with the trestatin A derived pseudooctosaccharide V-1532 (Machius et al., 1996), and its complex with the microbial inhibitor Tendamistat (Wiegand et al., 1995).

Comparisons between the binding segments of PPA identified in the known complexes have shown that the same main regions of PPA are always involved in the tight contacts. With regard to the CGTases, the X-ray structure of CGTase from *Bacillus circulans* strain 251 in complex with acarbose (Strokopytov et al., 1995) has been found to show similarities with the corresponding complexes with PPA; the acarbose binds near the catalytic residues. The acarviosine unit, which is the essential structural unit responsible for the activity of inhibitors of the acarbose type, does not bind across the site of hydrolysis however, contrary to what occurs in the amylase complexes.

Thiooligosaccharides are now becoming useful tools for structural studies on glycosyl hydrolases (Sulzenbacher et al., 1996; Driguez, 1997). The thio-linkage introduces some structural modifications into the sugar molecule, but X-ray data (Perez & Vergelati, 1984) and conformational studies (Bock et al., 1994) on methyl 4-thio- α -maltose have shown that its overall conformation is similar to that of the parent maltose residue and that this linkage has a high degree of flexibility. As was to be expected, methyl 4,4'-dithio- α -maltohexaose is not hydrolysed by porcine pancreatic α -amylase and has a K_i of 9 mM (Blanc-Muesser et al., 1992).

In the present study, the three-dimensional structure of native PPA soaked with a substrate analogue, methyl 4,4'-dithio- α -maltohexaose, was determined at 2.03 Å resolution. Our X-ray analysis showed a clearly visible pattern of electron density corresponding to trisaccharide molecules at four of the enzyme's substrate-binding subsites at the active site and to a ligand bound at the surface "second site" previously identified in the study by Qian et al. (1995). The electron density at subsite -1 was notably weaker than that observed at the other subsites and was modeled with water molecules.

Results

Quality of the model and difference electron density map

At 1σ level in the final $(2F_{obs} - F_{calc})\exp(i\alpha_{calc})$ map, all the atoms in the model have a well-defined density, except for a few

side chains as previously mentioned in the PPA maltopentaose complex, and two additional side chains from residues Asn53 and Glu352. These two side chains are located close to ligand-binding residues; depending on the structural changes induced by the ligand binding, neighboring residue side chains are variably stabilized in the structures. As observed in the structure of PPA in complex with a maltopentaose substrate, the interaction with the substrate analogue induces more strongly defined densities in the case of most of the residues than in the uncomplexed PPA structure. In particular, all the atoms at the N-terminal end are perfectly defined and an excellent density is observed corresponding to the pyrrolidone ring formed by the Gln1 residue we previously identified in the structures of pig pancreatic α -amylase isozyme I (Qian et al., 1995) and II (Gilles et al., 1996). All the protein residues directly contacting the bound ligand are very clearly observed in the electron density maps as are the water molecules.

The bound ligand—At the active site

Initial difference Fourier maps showed clear and unambiguous density corresponding to glucose rings Glc1, Glc2, Glc3, and Glc4 entering subsites labeled -3 , -2 , $+1$, and $+2$, respectively (nomenclature $-n/+n$ with cleavage taking place between subsites -1 and $+1$; Davies et al., 1997). Due to the shape of the density, it was possible to model two glucose units at subsites -3 and -2 , with subsite -2 accommodating the methyl glucoside residue. A region of density that cannot satisfactorily be modeled as solvent existed adjacent to the -3 subsite glucose unit; the interglycosidic sulfur atom and the C1 carbon of the non-reducing glucose unit of the trisaccharide molecule could be fitted into the density. The ($F_{obs} - F_{calc}$) map indicated the presence of this third residue, which probably became disordered in the solvent. A second trisaccharide molecule was easily fitted to the observed density at subsites $+1$ and $+2$, with its reducing end being disordered in the solvent. The sulfur atom of the 1–4 linkage between the sugar ring bound at subsite $+2$ and the postulated adjacent sugar was fitted

into the density. This density could not be satisfactorily modeled with a methyl group (and indeed, comfortably accommodates the sulfur atom), which indicates that there should be an additional glucose ring toward the reducing end, as actually suggested by the difference electron density maps. Each glucose residue was fitted to the electron density in a standard chair conformation (4C_1), the refinement was performed with full occupancy in each case, corresponding to reasonable individual atomic B values. The final density corresponding to the ligand is as strong as that of the surrounding active site atoms, all the atoms of the glucose units are visible. The final electron density map obtained is shown in Figure 1C.

Thermal parameters. The thermal parameters with the bound sugar ring atoms differ among subsites; the average B values obtained with the glucose units at subsites -3 , -2 , $+1$, and $+2$ are 27 , 15 , 32 , and 24 \AA^2 , respectively. This differs from the gradual change in the B values of the bound sugars previously observed in the structures of the PPA/acarbose complexes (Qian et al., 1994; Gilles et al., 1996). These structures showed that the atoms at external subsites exhibited the highest values, and that the mobility of the sugars in these ligands therefore increased toward the peripheries of the active site cleft. The low B-factor values obtained on the atoms of the glucose unit bound at subsite -2 and the very clear electron density associated with the methyl glucoside reflect the strength of the interaction in this binding region. The thermal parameters associated with the atoms of the glucose ring occupying subsite $+1$ exhibit the highest values; in the present complex, the sugar moiety is not strengthened by its connection with the unit occupying subsite -1 , contrary to what was observed in the PPA/acarbose complex, and makes remarkably few direct interactions with the protein (Table 1).

The cleavage site. A water molecule network occupies subsite -1 (Fig. 3). Six well-ordered water molecules could be easily accommodated into the density, four of which (W643, W748, W587, W566) were present in the free enzyme structure in the very

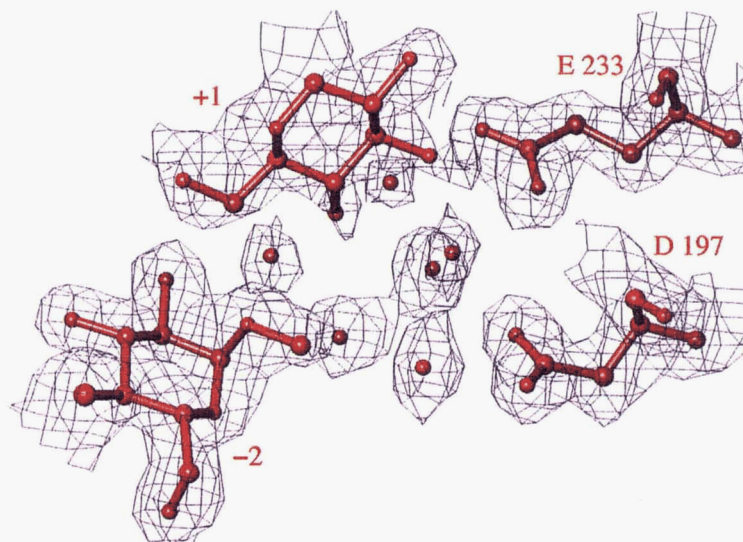


Fig. 3. $2F_{obs} - F_{calc}$ density map, contoured at the 1σ level, in the case of the PPA/SA complex in the vicinity of the active site. The water molecule network at the subsite -1 is visible. The catalytic residues, nucleophile, and acid catalyst (Asp197 and Glu233, respectively) are also shown.

Table 1. Protein-thio-oligosaccharide interactions in the PPA/SA complex

Sugar	Polar contacts with protein			Water-mediated polar contacts with protein					
	Site	Sugar atom	Protein atom	d (Å)	Sugar atom	Water	d (Å)	Water	Protein atom
Glc1	O5	Gln 63 NE2	3.3	O6	Ow666	2.8	Ow666	Gly 106 N	2.9
					S4	Ow937	3.1		
Glc2	O2	His 305 ND1	2.8	O1	Ow970 ^a	3.1			
		Trp 59 O	2.8	O2	Ow970 ^a	2.8			
		Gln 63 NE2	2.9	O3	Ow933 ^a	3.3			
Glc3	O2	His 201 NE2	2.8	O3	Ow986 ^a	2.9	Ow986 ^a	Glu233 OE1	2.6
				O4	Ow970 ^a	2.6	Ow950 ^a	Ow856	2.8
				O5	Ow950 ^a	3.3	Ow764	Gly 306 N	3.0
				O6	Ow950 ^a	2.6	Ow856 ^a	Tyr 151 OH	2.8
				O6	Ow764	2.8			
Glc4	O2	Glu 240 OE1	2.7						
	O2	Glu 240 OE2	3.2	O6	Ow856 ^a	3.1			
	O2	Lys 200 NZ	2.8	O6	Ow950 ^a	3.1			
	O3	Lys 200 NZ	2.8						
Glc5	O2	Glu 390 OE1	3.1	O4	Ow906 ^a	2.9	Ow906 ^a	Asp375 OD1	2.9
	O3	Arg 389 NH1	2.6	O4	Ow921	3.3	Ow921	Asp 375 O	3.1
	O5	Arg 389 N	3.2	O6	Ow925 ^a	2.9	Ow925 ^a	Ow921 ^a	3.0
	O6	Arg 389 N	3.1				Ow925 ^a	Arg 392 NH1	3.0
	O6	Arg 387 O	3.0						
Glc6	O2	Lys 322 NZ	3.0	S1	Ow931	3.1			
	O3	Lys 322 NZ	3.0	O2	Ow885 ^a	3.0			
				O6	Ow661	2.7			
				O6	Ow875	2.9			

^aPresent only in the complexed state.

central part of the catalytic cavity, firmly bound to the catalytic residues Glu233 and Asp197. Two additional water molecules (W970, W986) present in the current complex form strong hydrogen bonds with the carboxyl groups of Glu233 and Asp300.

Comparison with the acarbose-ligand binding

Upon superimposing the final ligands observed at the active site of the enzyme with the acarbose and present substrate analogue (Fig. 4) it is observed that, in both cases, the direction of the chain is the same. In the present complex, however, the glucose residues bound at subsites -3 and -2 are shifted slightly about 1.1 Å parallel to the C4-C1 direction toward the (non-reducing) entrance of the depression. At the opposite end, the glucose unit bound at subsite +2 remains in the same position, firmly bound by a subset of hydrogen bonds and the important contact with Tyr151. In comparison with the corresponding portion of the acarbose ligand, the present molecule bound at subsites +1 and +2 swings slightly around the reducing-end extremity, toward the solvent. The sugar unit bound at subsite +1 (close to the point of cleavage), which was previously located deeper into the cleft, clearly appears to have shifted outwards into the solvent filling the center of the V-shaped depression. It should be noted that the architecture of subsites +1 and +2 includes the flexible loop (residues 303-309; Qian et al., 1994), which forms the solvent-side edge of this binding region. In the present structure, the glucose bound at the leaving group subsite +1 is found to have shifted outward. This finding is in line with our previous suggestion (Qian et al., 1994) that in

the last stage of hydrolysis the release of the product from the active center may be accompanied by a loop movement.

The bound ligand—At the “second site”

The site henceforth referred to as the “second site” is located at the interface between the so-called domains A and C of the free-enzyme structure (notation according to Qian et al., 1993). Regardless of which oligosaccharide is used in the binding study (Payan et al., 1980; Qian et al., 1995; and the present study), two glucose units bind at this site, and the bound maltoside unit has the same conformation. The architecture is also similar: The maltoside disaccharide in an approximately helical conformation curls toward the protein, abutting against the aromatic side chain of the Trp388 residue, and then away. The final electron density map of the thio ligand obtained is given in Figure 5.

The glucose unit labeled Glc5 in the present study (Fig. 6) superimposes satisfactorily with the sugar unit 1A observed in the PPA/maltopentaose complex, whereas, because an S-linkage is present instead of the O-linkage between Glc5 and Glc6, ring Glc6 of the thiomaltosyl unit is shifted along (about 1 Å) with respect to the position of ring 2A in the maltose observed in the previous structure. The same protein ligands are involved in the interaction in both cases (Table 1). The architecture of the maltose-binding site, which shows the “classical” stacking pattern below a tryptophan residue (here Trp388), is completed by residues Glu390, Arg389, Arg387 (hydrogen-bonded to the hydroxyl groups of Glc5), and Lys322 (hydrogen-bonded in a bidentate mode to the hydroxyl

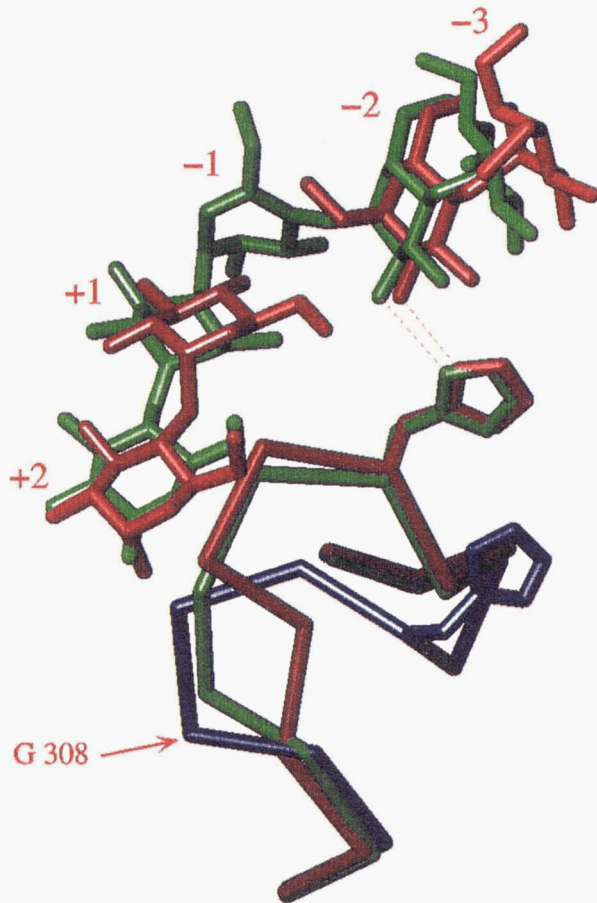


Fig. 4. Superimposition of the results obtained with acarbose (green) and substrate analogue (red) ligands at the active site of PPA. The superimposed α -carbon backbone traces obtained in the region of the flexible loop with free- (blue), acarbose-(green), and SA- (red) complexed PPA are also shown. The side-chain of His305 is shown with the three structures; in the two complexed states of PPA this side chain establishes the same strong hydrogen bond with the residue at subsite -2.

groups of Glc6) (Fig. 7A). The nonpolar cluster, C2-H, C4-H (residue Glc6) and C1'-H (residue Glc5), is stacked directly below the plane of the indole ring of Trp388, clearly establishing hydrophobic interactions. The tryptophan ring, polar side chains, and main-chain polar groups act as a platform associated with pincers serving to dock the thiomaltose. In the present study, as previously observed at the maltose binding site analyzed in the PPA/maltopentaose complex structure, the thiomaltose residue is further stabilized by a van der Waals interaction with residue Trp134 (domain B) of a contiguous symmetrical enzyme molecule. Depending on the size of the molecule, slight structural rearrangements occur (Fig. 6). Residues Glu484 and the latter residue Trp134 move in order to maintain the same configuration (as observed upon maltose binding) around the bound molecule; the side chain of Trp134 swings around its CA-CB bond and adopts a specific conformation maintaining van der Waals interaction with the bound sugar Glc6. In the present structure, the residue Glu484 moves away about 0.5 Å from its position in the native PPA structure, while in the PPA/maltopentaose complex, it moved in the opposite direction, about -0.5 Å. As a result, the approximate distance between Glu484-CA and the O2 hydroxyl of the glucose residue

(Glc6, in the present study and 2A in the PPA/Glc5 study), is invariable (about 8 Å). Likewise, the indole ring of Trp134 adopts in both the present and the PPA/maltopentaose complex structures nearly symmetrical positions versus its position in the native PPA structure.

Conformational parameters of the 4-thiooligosaccharides bound to the enzyme

The torsional angles Φ [O-5' - C-1' - S - C-4] and Ψ [C-1' - S - C-4 - C-3] that describe the relative orientation of the glucopyranose residues and the bond angle τ [C-1' - S - C-4] are analyzed in the three maltoside molecules Glc1-Glc2, Glc3-Glc4 and Glc5-Glc6 identified in the present structure (see Table 2). They are compared with the corresponding values calculated with the 15 local minima of methyl 4-thio- α -maltoside using PCILO (perturbed configuration interaction with localized orbitals) method (Mazeau & Tvaroska, 1992) and those based on the crystal structure of methyl 4-thio- α -maltoside (Pérez & Vergelati, 1984).

The values observed in the present structure lie in the regions of the minimum T15, T5, T7, T8 values in the PCILO energy surface map (Mazeau & Tvaroska, 1992) and are similar to the values based on the data by Pérez and Vergelati (1984).

It was pointed out by Mazeau and Tvaroska (1992) that in the case of methyl 4-thio- α -maltoside conformers ranging in the region of the minimum T5, T7, and T8 values of the PCILO energy surface, intramolecular hydrogen bonds occur between O2' and O3, which also occur in the crystal structure of α -(1,4)-O linked maltose. In the present structure, this hydrogen-bonding characteristic of the preferential geometry of maltose and amylose polymers (Johnson et al., 1988) is found to be conserved in the Glc3-Glc4 and Glc5-Glc6 structures.

Conformational changes in the enzyme

The overall conformation of PPA in the complex is essentially the same as in the native structure (Qian et al., 1993), with an average RMS deviation value of 0.38 Å. Large deviations are observed in the region between residues 303 and 309; this segment corresponds to the flexible loop identified in our previous free and acarbose-complexed PPA structures (Qian et al., 1993, 1994). However, the flexible loop, which is clearly defined, is found here to adopt a new specific conformation which differs from that observed with the acarbose ligand. The displacement of the loop, which occurs in response to the substrate analogue binding, can be seen in Figure 4. It moves toward the saccharide, thus reducing the

Table 2. Geometry of the glycosidic linkages

Structure	Φ^a (°)	Ψ^b (°)	τ^c (°)	PCILO ^d	O2'-O3 (Å)
Glc1-Glc2	111.8	-96.4	103.2	T15	
Glc3-Glc4	125.9	-119.5	99.9	T5-T7-T8	2.69
Glc5-Glc6	109.9	-158.0	104.9	T5-T7-T8	3.0
Methyl α -Thiomaltoside ^e	89.0	-116.8	100.3		

^a Φ is the torsion angle defined by [O-5'-C-1'-S-C-4].

^b Ψ is the torsion angle defined by [C-1'-S-C-4-C-3].

^c τ is the bond angle defined by [C-1'-S-C-4].

^dMazeau and Tvaroska (1992).

^eThe values are from Pérez and Vergelati (1994).

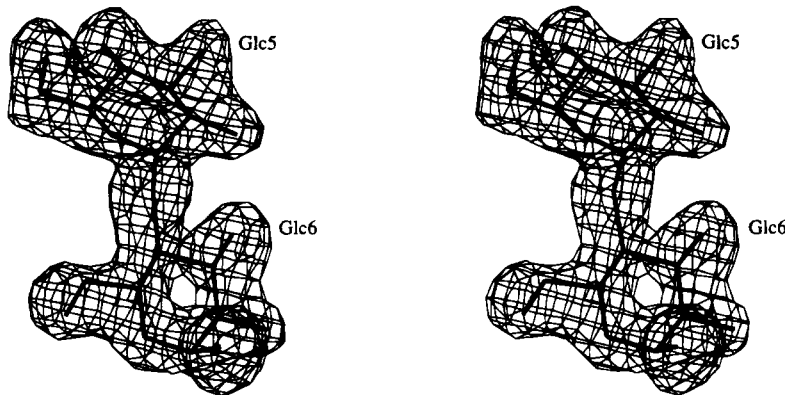


Fig. 5. Electron density map of the disaccharide bound at the "second site." Stereo view of an annealed omit SIGMAA-weighted map (Read, 1986); the contour level is at 3.0 times the RMS electron density of the map.

cleft breadth; the maximum main-chain movements recorded are 4.88 Å at His305–C α and 4.8 Å at Ala308–C α (Fig. 8). The motion around residue Ala308 gives rise to a specific conformation. As shown in Figure 4, a segment of the loop (303–305) superimposes with the corresponding region in the PPA/acarbose complex, and it is noteworthy that His305, which approaches the inhibitor from the solvent side, adopts the same position in both structures and makes the same strong hydrogen bond with the residue at subsite –2. The following part of the flexible loop deviates, on the contrary, from the previous track observed in the PPA/acarbose complex. Although it also deviates considerably from its path in the free enzyme, a similar β -turn structural element is conserved in the architecture. Upon acarbose binding, the configuration induced in this loop segment formed an extended cleft surface edge. As shown in Figure 4, the β turn does not involve the same residues in the present and free structures and in the region around residue Gly308, where the tracks in the free PPA and PPA/acarbose structure meet; here the flexible loop deviates from both

paths. It is henceforth obvious that, depending on the structure of the ligand, the moving loop adopts different conformations and participate strongly in the docking. The conformational changes described here are accompanied by a readjustment of the surrounding side chains, especially those in region of the neighboring loop (residues 351–359).

As shown in Figure 8, slight changes in the protein backbone are observed in the region of domain B, which includes the two cysteine residues Cys103 and Cys119. These changes are not due to the inhibitor binding but to the fact that, in the present structure, the two cysteine residues are bridged by a mercury atom and this induces slight structural changes in the surrounding region. Another noticeable difference is observed in the protein backbone in the region around residue 224: The previous structures of PPAI (Qian et al., 1993) and PPAII (Gilles et al., 1996) showed two opposite orientations of the carbonyl main-chain group of residues Ala224, whereas in the present complex the two configurations co-exist and the side chain is disordered.

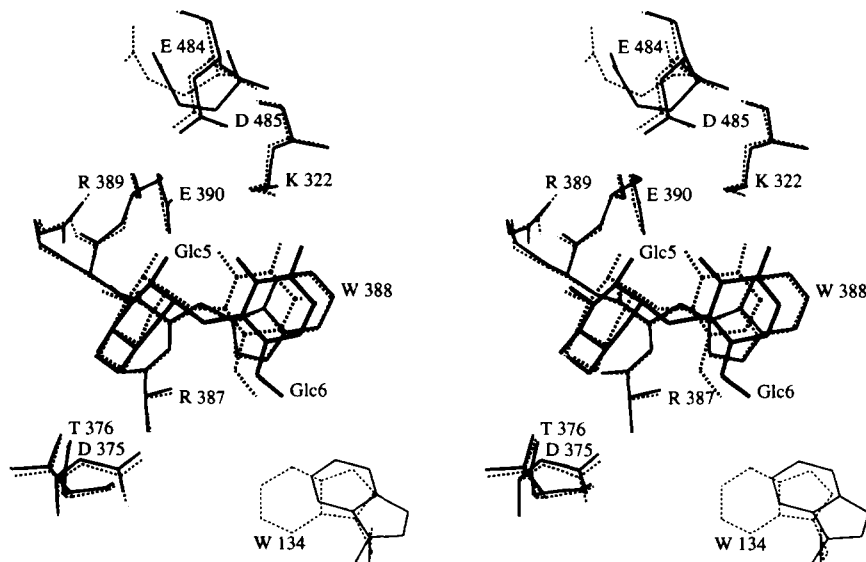
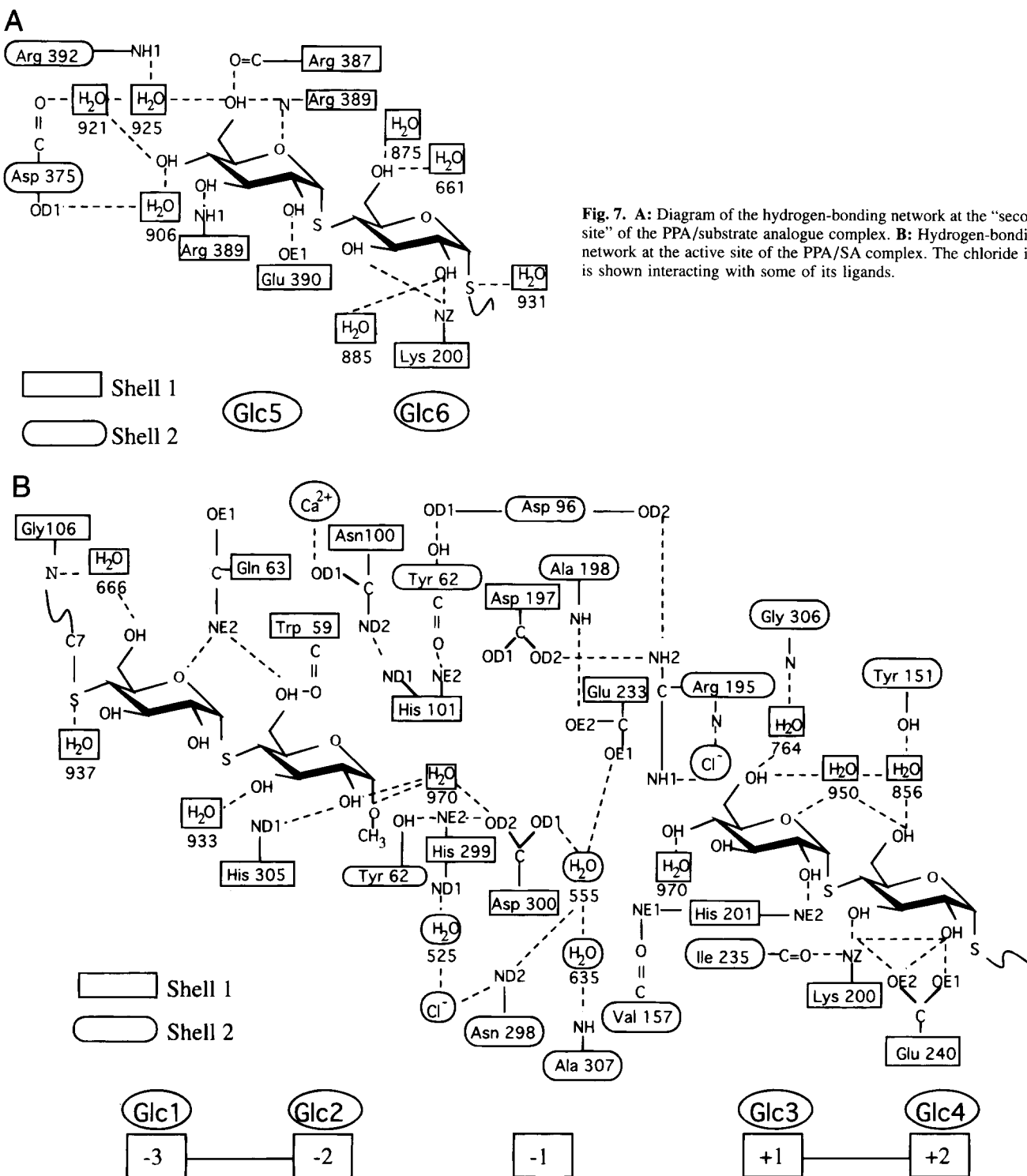


Fig. 6. Superimposed stereo views of the disaccharide maltose (Qian et al., 1995) and thiomaltose bound at the "second site."



Solvent structure

Upon comparing the free and complexed structures of PPA, it emerges that the motion of the flexible loop is accompanied by changes in the water molecule network extending from water molecule 555, close to the point of attack, to the bulk solvent. In the

PPA/acarbose complex, two structural water molecules, water 555 and water 635, formed a water bridge reaching from the catalytic center to the flexible loop (Ala307N). In the present structure, the flexible loop is found to have a different conformation and it is accompanied by a network of new water molecules connecting the

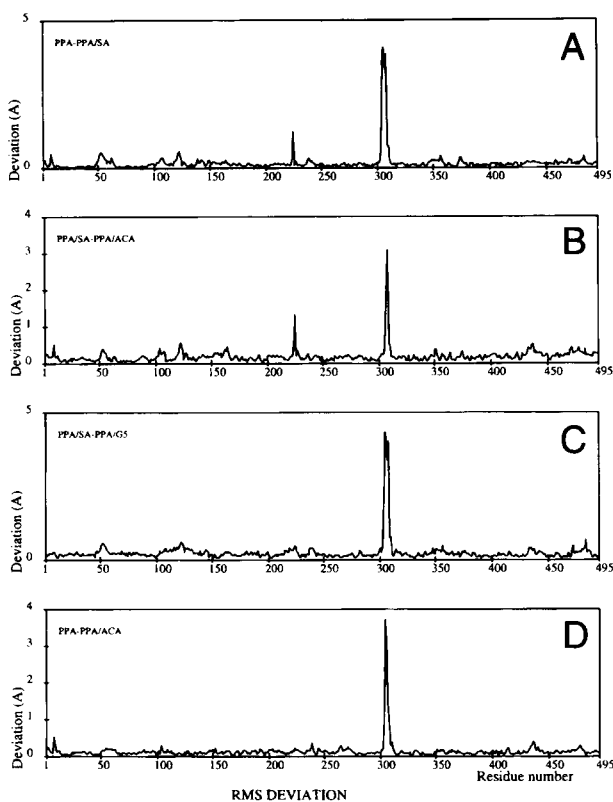


Fig. 8. RMS deviation between corresponding main-chain atoms of the free and complexed structures of PPA. **A:** Comparison between free and thio oligosaccharide-complexed PPA. Deviations corresponding to the “flexible loop” (303–309) show two maxima at residues His305 and Gly308. **B:** Present structure versus the PPA/acarbose complex structure (Qian et al., 1994); the differences between the conformations of the flexible loop particularly around Gly308 can be noted. **C:** Present structure versus the PPA/maltopentaose structure (Qian et al., 1995). **D:** Native structure as compared to the PPA/acarbose complex from Qian et al., (1994).

previous water bridge (555, 635) to the bulk solvent, which coincides and superimposes with the track taken by the flexible loop in the PPA/acarbose complex. The water channel runs from the point of attack to the bulk solvent.

Interactions in the active center

The enzyme makes both hydrophobic and hydrogen-bonding contacts with substrate analogue residues (Table 1; Fig. 7B).

Non-polar enzyme–carbohydrate interactions are observed with the aromatic residues lining the active site depression. The clear hydrophobic stacking of aromatic residues Trp58 and Trp59, previously observed in the PPA/acarbose complexes is conserved at subsites –3 and –2, where the indole ring of Trp59 is nearly parallel to the sugar surface. Tyr151 lies parallel to the surface of the glucose unit bound at subsite +2. At subsite +1, a similar interaction with side chains of Leu162 and Val163 is again observed.

Subsite –3 (I)

In comparison with the acarbose ligand binding, the sugar residue bound at subsite –3 is shifted toward the solvent (Fig. 4) and, as a result, the connections with the protein residues Val163 and

Leu165 are lost. An additional water-mediated hydrogen bond is observed between the O-6 hydroxyl group and the protein residue Gly106. The latter residue was present at the additional binding site (subsite –4) identified in the PPA/acarbose complex (Gilles et al., 1996) obtained with a different crystal form (72% solvent). The glucose ring is found in the present study to sit in an intermediate position between the subsites called 0 and I (here: –4, –3) in the PPA/acarbose complex. This finding shows that the interaction that takes place in the binding cleft is not a rigid one.

Subsite –2 (II)

Similar direct interactions between the protein and the sugar residue (Glc2) bound at subsite –2 are observed in the present study and in the PPA/acarbose complexes. The shifting of unit Glc2 observed in the present study is accompanied by a slight movement of the surrounding protein ligands and in particular the side chain of Trp59 moves some 0.5 Å from its position in the acarbose complexes in order to trigger the interaction.

Subsite +1 (IV)

The +1 subsite glucose participates in remarkably few direct interactions with the protein. The O2 hydroxyl makes a direct hydrogen bond with the enzyme residue His201. This histidine residue was involved in the acarbose inhibitor binding and formed a strong hydrogen bond with the O2 of the amino sugar. The O6 hydroxyl forms a water-mediated hydrogen bond with the amide group of Gly306 from the flexible loop; the presence of the hydroxyl group at the C-6 atom, which was missing from the amino sugar of the acarbose inhibitor is probably important. In the PPA/acarbose complex, Gly306 interacted with the glucose ring bound at subsite +2. In the present study, the residue switches its hydrogen bonding from subsite +2 to subsite +1. This interaction with the moving loop contributes to the conformational change and may be necessary to the product release. The oxygen ring O5 forms water-mediated hydrogen bonds with Tyr151. The glucose ring bound at this subsite has lost the links with the catalytic residues Asp300 and Glu233, which are present in the acarbose ligand. The paucity of the interactions at this leaving group subsite presumably is correlated with the product-release process in the hydrolysis pathway.

Subsite +2 (V)

The sugar at subsite +2 is held by hydrogen bonds with protein residues Lys200 and Glu240 as previously observed, but in the current study, residue Glu240 is hydrogen bonded in a bidentate mode to the O2 hydroxyl. The side chain of this residue adopts slightly different conformations in the known free and complexed structures of PPA. On one side of the glucopyranose ring, the hydrophobic patch composed of C2 and C4 stacks within 4 Å of the atoms from the aromatic ring of Tyr151.

Subsite –1(III)

The water molecule network occupying the catalytic subsite is found to provide strong hydrogen bonds with some of the main residues: Glu233, Asp197, Asp300, His299, Arg195.

Discussion

Small substrates such as maltotriose can establish a large number of possible binding interactions with PPA (Robyt & French, 1970).

The crystal may be composed of a mixture of states reflecting an equilibrium under the conditions of crystallization, giving rise to some heterogeneity in the binding scheme of the thiomaltotriose molecules. In the present structure, the binding of the substrate analogue may involve a series of overlapping networks, which, depending on the affinity of the subsites, produce variably strong electron density patterns. The lowest temperature factor values are those recorded in the case of the glucose units modeled at subsites -2 and +2, and the predominant electron density pattern here seems to correspond to the binding of thiomaltotriose molecules at subsites (-4) -3, -2, and at subsites +1, +2 (+3).

The dithiomaltotriose molecule is not cleaved by α -amylase and a K_i of 9 mM was obtained (Blanc-Muesser et al., 1992). A Hg-soaked crystal was used in our study. It is theoretically possible that, under specific conditions, interactions between the methyl 4,4' dithio- α -maltotrioside and HgCl₂ may lead to the formation of glucose molecules (see Materials and methods); thioglycosidic bonds are also known to be unstable in the presence of HgCl₂ at high concentrations (Raymond, 1945).

The electron density observed at the surface binding site and at the subsites prior to and subsequent to the site of cleavage (active binding site) is not consistent with the presence of hydrolyzed molecule in the complex structure.

The electron density patch at subsite -1 is notably weaker than that observed at the other subsites. This pattern of density was modeled with water molecules. There exists a possibility, however, that the -1 sugar may be disordered. In this case, a possible explanation might be that some molecules in the overlapping network may have bound substrate analogue molecules spanning the point of enzymatic cleavage. Although hydrolysis seems extremely unlikely to have occurred within the crystal, it is possible that a cleavage product might have bound. The lack of significantly strong electron density levels indicates that if any binding modes of this kind did occur, they could not account for a significantly large fraction of the molecules. The glucosyl unit preceding the cleavage site probably binds rather poorly.

It is worth noting that if the binding of dithiomaltotriose molecule to subsites -3 and -2 gives rise to a well-ordered density with higher B values at the external subsites, the binding to the "leaving group subsites" and to the catalytic subsite reflects much more complicated interactions. The B values of flanking atoms of Glc2 and Glc3 adjacent to the catalytic subsite (-1) differ: the O1 atom of Glc2 has a B value of 14 Å², whereas the O4 atom of Glc3 gives a B value of 30 Å². The atoms at subsite +1, exhibit the highest B values, averaging 29 Å², as compared with 22 Å² in the case of atoms belonging to the glucose unit occupying the external subsite +2. This suggests that the stacking of Tyr151 against the sugar at subsite +2 may be part of a specific substrate recognition process. The lack of distinct density patches observed at the point of cleavage with this substrate analogue might be taken to support the idea that enzymes have evolved in such a way that they bind to the transition states of substrates more strongly than to the substrates themselves.

Materials and methods

A crystal of bridged mercurial derivative S103-HG-S119 prepared by performing co-crystallization in the presence of HgCl₂ was used in this study. Crystals of the substrate analogue (SA) complex were isomorphous to those of the native enzyme. The methyl 4,4' dithio- α -maltotrioside shown in Figure 1B was obtained as previously

described (Blanc-Muesser et al., 1992). It has been found that 12 h incubation of a mixture of this compound and HgCl₂ (1:2 w/w) may have favored the formation of glucose molecules (H. Driguez, unpubl. results). The crystal packing (Payan et al., 1980) allows the study of substrate interactions with the enzyme by soaking native crystals in buffered crystal-stabilizing solutions of the compound of interest. In the present study, complexes were formed by soaking crystals for 10 h at 20 °C in a solution containing 10 mM of the compound in Tris buffer 0.01 M, 1 mM CaCl₂ 2 M NaCl at pH 8. X-ray diffraction data on the substrate analogue complex crystals were collected using a Mar-Research imaging plate scanner developed by Hendrix and Lentfer, Hamburg. The data were processed and scaled with the programs DENZO and SCALEPACK (Otwinowski, 1993). The data set used with the SA complex was 99.4% complete up to 2.03 Å resolution and 88.1 % complete in the final shell with I/σ above 3.0. The data collection statistics are given in Table 3.

The $(F_{obs,complex} - F_{obs,native})\exp(i\alpha_{calc,native})$ maps calculated between 35 and 2.03 Å showed clear density corresponding to a disaccharide ligand in the so-called "second" binding site described by Qian et al. (1995). An extremely clear-cut pattern of density corresponding to four fully occupied subsites was observed at the active-site depression on both sides of the catalytic subsite; in the catalytic center, the observed density was not as strong as at

Table 3. Data collection and refinement statistics

	Complex	
Cell parameters (P2 ₁ 2 ₁ 2 ₁)		
<i>a</i> (Å)	56.3	
<i>b</i> (Å)	87.8	
<i>c</i> (Å)	103.4	
Resolution limit (Å)	2.03	
No. of measurements	322,368	
Unique reflections	33,718	
% of data > 1 σ (overall/last shell) ^a	99.4/99.8	
% of data > 3 σ (overall/last shell) ^a	95.3/88.1	
R_{sym} ^b (overall/last shell) ^a	5.7/13.9	
Refinement range (Å)	35–2.03	
No. of reflections in refinement	33,421	
<i>R</i> -factor (%) ^c	16.0	
R_{free} ^d	18.5	
No. of protein atoms	3908	
No. of ligand atoms	71	
No. of water molecules	384	
RMS deviations	Protein	Ligand
Bond lengths (Å)	0.010	0.013
Angles (°)	1.4	2.0
Temperature factors $\langle B \rangle$ (in Å ²)		
Main-chain atoms	13.6	—
Side-chain atoms	18.5	27.5
Water molecules	34.3	—

^aOverall data: 40–2.03 Å; last shell 2.07–2.03 Å.

^b R_{sym} is defined as $\sum_{i,hkl} |I(i,hkl) - \langle I(i,hkl) \rangle| / \sum_{i,hkl} I(i,hkl)$ where *i* runs through the symmetry-related reflections.

^cThe crystallographic *R* is defined as $\sum |F_o - F_c| / \sum |F_o|$.

$$\text{d}R_{free} = \frac{\sum_{(h,k,l) \in T} ||F_{obs}(h,k,l) - k|F_{calc}(h,k,l)|}{\sum_{(h,k,l) \in T} |F_{obs}(h,k,l)|}.$$

the other subsites. The initial phases of the complex ($\alpha_{calc,native}$) were calculated from the completely refined model for the native enzyme (Qian et al., 1993).

Refinement was performed using the XPLOR slow-cooling protocol (Brünger et al., 1987), using all the data recorded between 35 and 2.03 Å. It was followed by manual rebuilding into SIGMAA-weighting (Read, 1986) electron density maps with the TURBO-FRODO graphics program implemented on a Silicon graphics 4D/380 computer (Roussel & Cambillau, 1989). As all the data recorded were employed in the refinement, a low-resolution bulk solvent correction, as implemented in the XPLOR program version 3.843 (Brünger, 1996), was applied. The behavior of R_{free} was monitored (Brünger, 1992).

The procedure was carried out starting with the refined structure of uncomplexed PPA, deleting number of water molecules which overlapped with the observed initial difference Fourier density in the region of the active site and that of the second binding site. The template of a glucose residue for refinement of the ligand structure was taken from crystallographic data for individual monosugars. Any solvent molecules with densities below 1σ in the $(F_{obs} - F_{calc})\exp(i\alpha_{calc})$ map and temperature factors above 55 Å² were removed after the first refinement iteration. The difference electron density map also showed the presence of additional water molecules, although some of the ordered molecules previously present in the free enzyme structure had disappeared; sites were added to the model whenever the electron density level was at least 3.5σ in the $(F_{obs} - F_{calc})\exp(i\alpha_{calc})$ maps. The molecules introduced were inspected visually to check whether the hydrogen-bonding geometry was correct, and they were given an initial *B*-factor of 20 Å². No oligosaccharide atoms were included in the refinement until the refinement of the protein had reached convergence and the sugar density pattern was clear-cut. During the XPLOR *B* value refinement procedure, the oligosaccharide molecules were refined with no restraints on the *B* value.

Based on the shape of the electron density a thiomaltose residue was identified at the "second site" and two separate thiomaltose residues were located at subsites -3 to -2 and +1 to +2 of the active site, respectively. At first only these three maltoside units were introduced into the refinement procedure. The electron density observed at subsite -1 was modeled in the last stages of the refinement. A network of water molecules accounted satisfactorily for the observed density.

When the *R*-factor had reached 16.0% in the 35.0 to 2.03 Å range for 33,421 reflections with a model obeying standard geometry within 0.011 Å in bond lengths and 1.4° in bond angles, and the $(F_{obs} - F_{calc})\exp(i\alpha_{calc})$ map was no longer showing any interpretable features, the refinement procedure was ended. Based on the Luzzatti plots obtained using the free *R*-factor (Luzzatti, 1952), the upper estimate of the error in the atomic positions is 0.2 Å. The final model consists of 3908 protein atoms (i.e., all non-hydrogen atoms), 1 Ca ion, 1 Cl ion, 1 Hg atom, 71 oligosaccharide atoms, and 384 water molecules.

Acknowledgments

This work has been funded by the CNRS and the Programme de Recherches Avancées de Coopérations Franco-Chinoises (PRA B95-4, Etudes Structurales) (M.Q. & F.P.). The authors thank Professor Tang, Peking University, for his helpful support. We are grateful to Dr. C. Cambillau and Dr. P. Alzari for helpful discussions. We thank P. Cantau and C. Carranza for their technical assistance.

References

- Alkazaz M, Desseaux V, Marchis-Mouren G, Payan F, Forest E, Santimone M. 1996. The mechanism of porcine pancreatic α -amylase kinetic evidence for two additional carbohydrate-binding sites. *Eur J Biochem* 241:787-796.
- Blanc-Muesser M, Vigne L, Driguez H, Lehmann J, Steck J, Urbahns K. 1992. Spacer-modified disaccharide and pseudo-trisaccharide methyl glycosides that mimic maltotriose, as competitive inhibitors for pancreatic alpha-amylase: A demonstration of the "clustering effect." *Carbohydr Res* 224:59-71.
- Bock K, Duus JO, Refn S. 1994. Conformational equilibria of 4-thiomaltose and nitrogen analogues of maltose in aqueous solutions. *Carbohydr Res* 253:51-67.
- Bompard-Gilles C, Rousseau P, Rougé P, Payan F. 1996. Substrate mimicry in the active center of a mammalian α -amylase: Structural analysis of an enzyme-inhibitor complex. *Structure* 4:1441-1452.
- Brayer GD, Luo Y, Withers SG. 1995. The structure of human pancreatic α -amylase at 1.8 Å resolution and comparison with related enzymes. *Protein Sci* 4:1730-1742.
- Brünger AT, Kuriyan J, Karplus M. 1987. Crystallographic R factor refinement by molecular dynamics. *Science* 35:458-460.
- Brünger AT. 1992. Free R value: A novel statistical quantity for assessing the accuracy of crystal structures. *Nature* 355:472-475.
- Brünger AT. 1996. *XPLOR version 3.843 Manual*. New Haven, Connecticut: Yale University Press.
- Cozzzone P, Pasero L, Marchis-Mouren G. 1970. Characterization of porcine pancreatic isoamylases: Separation and amino acid composition. *Biochim Biophys Acta* 200:590-593.
- Davies GJ, Wilson KS, Henrissat B. 1997. Nomenclature for sugar-binding subsites in glycosyl hydrolases. *Biochem J* 321:557-559.
- Driguez H. 1997. Thiooligosaccharides in glycobiology. In: Driguez H, Thiem J, eds. *Topics in current chemistry* 187. Berlin: Springer-Verlag. pp 85-116.
- Gilles C, Astier JP, Marchis-Mouren G, Cambillau C, Payan F. 1996. Crystal structure of pig pancreatic α -amylase isoenzyme II, in complex with the carbohydrate inhibitor acarbose. *Eur J Biochem* 238:561-569.
- Henrissat B. 1991. A classification of glycosyl hydrolases based on amino acid sequence similarities. *Biochem J* 280:309-316.
- Ishikawa K, Matsui I, Kobayashi S, Nakatani H, Honda K. 1993. Substrate recognition at the binding site in mammalian pancreatic α -amylases. *Biochemistry* 32:6259-6265.
- Johnson LN, Cheetham J, McLaughlin JP, Acharya KR, Barford D, Phillips DC. 1988. Protein-oligosaccharides interactions: Lysozyme, phosphorylase, amylases. *Curr Topics Microbiol Immunol* 139:82-134.
- Kluh L. 1981. Amino acid sequence of hog pancreatic α -amylase isoenzyme I. *FEBS Lett* 136:231-234.
- Koshland DE. 1953. Stereochemistry and the mechanism of enzymatic reactions. *Biol Rev* 28:416-436.
- Kraulis PJ. 1991. MOLSCRIPT: A program to produce both detailed and schematic plots of protein structures. *J Appl Crystallogr* 24:946-950.
- Levitzki A, Steer ML. 1974. The allosteric activation of mammalian α -amylase by chloride. *Eur J Biochem* 41:171-180.
- Luzzatti PV. 1952. Traitement statistique des erreurs dans la détermination des structures cristallines. *Acta Crystallogr* 5: 802-810.
- Machiusi M, Vertes L, Huber R, Wiegand G. 1996. Carbohydrate and protein-based inhibitors of porcine pancreatic α -amylase: Structure analysis and comparison of their binding characteristics. *J Mol Biol* 260:409-421.
- Mazeau K, Tvaroska I. 1992. PCILQ quantum-mechanical relaxed conformational energy map of methyl 4-thio- α -maltose in solution. *Carbohydr Res* 225:27-41.
- Marchis-Mouren G, Desseaux V. 1989. Structure and function of α -amylases. *Biochem Life Sci Adv* 8:91-96.
- McCarter JD, Withers SG. 1994. Mechanisms of enzymatic glycoside hydrolysis. *Curr Opin Struct Biol* 4:885-892.
- McCarter JD, Withers SG. 1996. Unequivocal identification of Asp-214 as the catalytic nucleophile of *Saccharomyces cerevisiae* α -Glucosidase. Using 5-fluoro glycosyl fluorides. *J Biol Chem* 271:6889-6894.
- Otwinski Z. 1993. Oscillation Data Reduction Program. In: Sawyer L, Isaacs N, Burley S, eds. *Proceedings of the CCP4 study weekend: Data collection and processing*. Warrington, United Kingdom: Daresbury Laboratory. pp 56-62.
- Pasero L, Mazzei-Pierron Y, Abadie B, Chicheportiche Y, Marchis-Mouren G. 1986. Complete amino acid sequence and location of the five disulfide bridges in protein pancreatic α -amylase. *Biochim Biophys Acta* 869:147-157.
- Payan F, Haser R, Pierrot M, Frey M, Astier JP, Abadie B, Duée E, Buisson G. 1980. The three-dimensional structure of α -amylase from porcine pancreas at 5 Å resolution. *Acta Crystallogr B36:416-421*.

- Pérez S, Vergelati C. 1984. Structure and conformational analysis of methyl α -thiomaltoside. *Acta Crystallogr B40*:294–299.
- Prodanov E, Seigner C, Marchis-Mouren G. 1984. Subsite profile of the active center of porcine pancreatic α -amylase. Kinetic studies using maltooligosaccharides as substrates. *Biochem Biophys Res Commun* 122:75–81.
- Qian M, Haser R, Payan F. 1993. Structure and molecular model refinement of pig pancreatic α -amylase at 2.1 Å resolution. *J Mol Biol* 231:785–799.
- Qian M, Buisson G, Duée E, Haser R, Payan F. 1994. The active center of a mammalian α -amylase. Structure of the complex of a pancreatic α -amylase with a carbohydrate inhibitor refined to 2.2 Å resolution. *Biochemistry* 33:6284–6294.
- Qian M, Haser R, Payan F. 1995. Carbohydrate binding sites in a pancreatic α -amylase-substrate complex, derived from X-ray structure analysis at 2.1 Å resolution. *Protein Sci* 4:747–755.
- Ramasubbu N, Paloth V, Luo Y, Brayer GD, Levine MJ. 1996. Structure of human salivary α -amylase at 1.6 Å resolution: Implications for its role in the oral cavity. *Acta Crystallogr D* 52:435–446.
- Raymond AL. 1945. Thio-and seleno-sugars. *Adv Carbohydr Chem* 1:129–145.
- Read RJ. 1986. Improved Fourier coefficients for maps using phase from partial structure with errors. *Acta Crystallogr A42*:140–149.
- Robyt JF, French D. 1970. The action pattern of porcine pancreatic α -amylase in relationship to the substrate binding site of the enzyme. *J Biol Chem* 245:3917–3927.
- Roussel A, Cambillau C. 1989. In: Silicon Graphics, ed. *Silicon Graphics geometry partner directory (Fall 1989)*. Mountain View, California: Silicon Graphics. pp 77–78.
- Steer M, Levitzki A. 1973. The metal specificity of mammalian α -amylases as revealed by enzyme activity and structural probes. *FEBS Lett* 31:89–92.
- Strokopytov B, Penninga D, Rozeboom J, Kalk KH, Dijkhuizen L, Dijkstra BW. 1995. X-ray structure of cyclodextrin glycosyltransferase complexed with acarbose. Implication for the catalytic mechanism of glycosidases. *Biochemistry* 34:2234–2240.
- Sulzenbacher G, Driguez H, Henrissat B, Schülein M, Davies GJ. 1996. Structure of the *Fusarium oxysporum* Endoglucanase I with a nonhydrolyzable substrate analogue: Substrate distortion gives rise to the preferred axial orientation for the leaving group. *Biochemistry* 35:15280–15287.
- Svensson B. 1994. Protein engineering in the α -amylase family: catalytic mechanism, substrate specificity, and stability. *Plant Mol Biol* 25:141–157.
- Vallee BL, Stein EA, Summerwell WN, Fisher EH. 1959. Metal content of α -amylases of various origins. *J Biol Chem* 234:2901–2929.
- Wakim J, Robinson M, Thoma JA. 1969. The active site of porcine pancreatic α -amylase: Factor contributing to catalysis. *Carbohydr Res* 10:487–503.
- Wiegand G, Epp O, Huber R. 1995. The crystal structure of porcine pancreatic α -amylase in complex with the microbial inhibitor Tendamistat. *J Mol Biol* 247:99–110.